Rheol Acta (2014) 53:791–804
DOI 10.1007/s00397-014-0803-1

ORIGINAL CONTRIBUTION

Numerical study of the combined effects of inertia, slip, and compressibility in extrusion of yield stress fluids

Zacharias Kountouriotis · Georgios C. Georgiou · Evan Mitsoulis

Received: 19 April 2014 / Revised: 17 August 2014 / Accepted: 5 September 2014 / Published online: 8 October 2014

Abstract The axisymmetric extrudate swell flow of a compressible Herschel–Bulkley fluid with wall slip is solved numerically. The Papanastasiou-regularized version of the constitutive equation is employed, together with a linear equation of state relating the density of the fluid to the pressure. Wall slip is assumed to obey Navier's slip law. The combined effects of yield stress, inertia, slip, and compressibility on the extrudate shape and the extrudate swell ratio are analyzed for representative values of the power-law exponent. When the Reynolds number is zero or low, swelling is reduced with the yield stress and eventually the extrudate contracts so that the extrudate swell ratio reaches a minimum beyond which it starts increasing asymptotically to unity. Slip suppresses both swelling and contraction in this regime. For moderate Reynolds numbers, the extrudate may exhibit necking and the extrudate swell ratio initially increases with yield stress reaching a maximum; then, it decreases till a minimum corresponding to contraction, and finally, it converges asymptotically to unity. In this regime, slip tends to eliminate necking and may initially cause further swelling of the extrudate, which is suppressed if slip becomes stronger. Compressibility was found to slightly increase swelling, this effect being more pronounced for moderate yield stress values and wall slip.

Keywords Herschel–Bulkley fluids · Yield stress · Extrusion · Extrudate swell · Reynolds number · Navier slip · Compressibility

Research highlights • The combined effects of inertia, slip, and compressibility in extrudate swell flow of yield stress fluids are investigated.
• Interesting extrudate shapes due to the competition of inertia and yield stress
• Slip may enhance swelling at moderate Reynolds numbers.
• Compressibility effects are found to be more pronounced for moderate yield stress values and wall slip.

Z. Kountouriotis · G. C. Georgiou (✉)
Department of Mathematics and Statistics, University of Cyprus, PO Box 20537, 1678 Nicosia, Cyprus
e-mail: georgios@ucy.ac.cy

E. Mitsoulis
School of Mining Engineering and Metallurgy, National Technical University of Athens, 15780 Zografou, Athens, Greece

Introduction

The extrudate swell flow is a well-known benchmark problem in the rheological community, characterized by the presence of a free surface and a boundary stress singularity at the die exit. This flow has been studied both experimentally on many different materials, such as polymer melts and pastes, and numerically for different (e.g., generalized Newtonian and viscoelastic) constitutive equations with a variety of numerical methods. Nevertheless, swelling is observed only at low Reynolds numbers, i.e., beyond a critical Reynolds number, the extrudate actually contracts (Omodei 1980; Georgiou et al. 1988; Georgiou and Boudouvis 1999). In Newtonian flow, the extrudate swell ratio, χ, defined as the ratio of the final extrudate radius to that of the die, is a decreasing function of the Reynolds number approaching asymptotically the limit for inviscid flow, which actually corresponds to contraction rather than to swelling, since it is less than unity (Georgiou et al. 1988). In other words, inertia tends to reduce swelling. This is not the case with slip, which reduces swelling at low and contraction at higher Reynolds numbers (Silliman and Scriven 1980; Kountouriotis et al. 2013). Hence, inertia and slip effects on the extrudate surface are similar at low and competing at higher Reynolds numbers. The numerical simulations of Kountouriotis et al. (2013) for the Newtonian flow demonstrated that this competition leads to interesting stable extrudate shapes at moderate slip and Reynolds numbers.

Compressibility is another factor affecting the extrudate swell ratio. In the case of Newtonian flow at low Reynolds numbers, it is well established that this ratio initially decreases slowly and then increases rapidly with compressibility, i.e., it passes through a minimum (Mitsoulis et al. 2012). Hence, beyond this minimum compressibility enhances swelling opposing inertia effects. Kountouriotis et al. (2013) investigated the combined effects of compressibility, Navier slip, and inertia on the shape of the Newtonian extrudate and found that at low Reynolds numbers, slip reduces swelling and alleviates compressibility effects: the extrudate swell ratio decreases (initially) more slowly with compressibility, and the minimum is moved to the right. At higher Reynolds numbers, the jet contracts at low and expands at higher compressibility values. Moreover, compressibility at moderate Reynolds numbers leads to stable steady states in which the extrudate surface exhibits oscillations that decay downstream and are suppressed by slip (Kountouriotis et al. 2013; Taliadorou et al. 2008).

In the present work we focus on the extrudate swell flow of fluids with yield stress. The class of yield stress or viscoplastic fluids includes a wide range of materials of industrial importance (slurries, pastes, suspensions, gels, semisolids, foams, food products, nanocomposites, waxy crude oil, well drilling fluids, and others). As pointed out by Rabideau et al. (2010), the extrusion behavior of pasty (i.e., yield stress) materials is much less well known than that of polymers. Our objective is to investigate the combined effects of inertia, slip, and compressibility in the axisymmetric viscoplastic extrudate swell flow.

The main feature of yield stress materials is that they do not deform when subjected to a stress below the yield stress, $\tau 0$. The simplest constitutive equation with a yield stress is the Bingham model, introduced by Bingham (1922). The Herschel–Bulkley model is the combination of the Bingham model with the power-law model, which accounts for shear-thinning or shear-thickening effects. In incompressible flow, this is written as follows:

$$\begin{cases} \dot{\boldsymbol{\gamma}} = \mathbf{0}, & \tau \le \tau_0 \\ \boldsymbol{\tau} = \left(\dfrac{\tau_0}{\dot{\gamma}} + k\dot{\gamma}^{n-1} \right) \dot{\boldsymbol{\gamma}}, & \tau > \tau_0 \end{cases} \tag{1}$$

where k is the consistency index, n is the power-law exponent, $\boldsymbol{\tau}$ is the stress tensor, and $\dot{\boldsymbol{\gamma}}$ is the rate-of-strain tensor:

$$\dot{\boldsymbol{\gamma}} = \nabla \mathbf{u} + (\nabla \mathbf{u})^T \tag{2}$$

$\mathbf{u}$ being the velocity vector and $\nabla \mathbf{u}$ the velocity-gradient tensor. The magnitudes of $\dot{\boldsymbol{\gamma}}$ and $\boldsymbol{\tau}$, denoted by $\dot{\gamma}$ and τ, respectively, are defined by $\dot{\gamma} \equiv \sqrt{II_{\dot{\gamma}}/2} = \sqrt{\dot{\boldsymbol{\gamma}} : \dot{\boldsymbol{\gamma}}/2}$ and $\tau \equiv \sqrt{II_{\tau}/2} = \sqrt{\boldsymbol{\tau} : \boldsymbol{\tau}/2}$ where II denotes the second invariant of a tensor. Setting $n=1$ in Eq. (1), we recover the Bingham model; in this case, k represents the plastic viscosity. The Bingham model is reduced to the Newtonian model when the yield stress is zero.

A difficulty that arises when solving flows of fluids obeying a two-branch constitutive equation is the need of determining the regions where either branch of the equation is applied, i.e., the so-called unyielded ($\tau \le \tau_0$) and yielded regions ($\tau > \tau_0$). This task may be trivial in the case of steady, one-dimensional flows amenable to analytical solutions. However, it becomes extremely difficult in transient one-dimensional flows or in steady two- or three-dimensional flows. There are two main approaches in tackling this problem. The first is the regularization of the constitutive equation so that the same expression is valid uniformly for any value of $\dot{\gamma}$. The second is based on the use of augmented Lagrangian methods (ALMs).

Regularization methods are easily implemented on existing, validated codes. The most popular regularization is the one proposed by Papanastasiou (1987) originally for the Bingham plastic. This was extended to the Herschel-Bulkley model by Ellwood et al. (1990), as follows:

$$\boldsymbol{\tau} = \left[\tau_0 \frac{1 - \exp\left(-m\dot{\gamma}\right)}{\dot{\gamma}} + k\dot{\gamma}^{n-1} \right] \dot{\boldsymbol{\gamma}} \tag{3}$$

where m is a stress growth parameter. Equation (3) approximates Eq. (1) for sufficiently large values of m. Once a viscoplastic flow is solved by means of Eq. (3), the interface of yielded/unyielded regions can approximately be tracked down a posteriori by using the criterion $\tau = \tau_0$ (Mitsoulis 2007). The Papanastasiou regularization has been employed by different groups in solving various viscoplastic flows [see Mitsoulis (2007) and references therein]. The method is known to exhibit convergence difficulties at high values of m and may lead to inaccurate results (Frigaard and Nouar. 2005). However, it performs very well for low and moderate yield stress values. The Papanastasiou as well as other regularization models used in the literature have been reviewed by Frigaard and Nouar (2005).

An alternative method to solve the aforementioned problems is the ALM developed by Fortin and Glowinski (1983). The advantage of that method is the accurate prediction of yielded and unyielded regions due to the use of variational inequalities, either rate-of-strain minimization or stress maximization. However, augmented Lagrangian methods are more complex, difficult to implement, and computationally costly (Glowinski and Wachs 2011; Dimakopoulos et al. 2013). Both augmented Lagrangian and regularization methods have been applied successfully to the numerical solution of various flows

(Glowinski and Wachs 2011). Their pros and cons are summarized in the recent review article of Balmforth et al. (2014) who note that "pragmatically, the choice between augmented Lagrangian and regularization is related to whether one needs to determine the position of the yield surface, or whether a reasonable approximation to the velocity field is sufficient."

In his pioneering paper where he introduced his regularized equation, Papanastasiou (1987) presented preliminary results for the creeping, planar extrudate swell flow of a Bingham plastic showing that swelling is reduced with the yield stress. The same conclusion was reached by Beverly and Tanner (1989) who analyzed the effects of yield stress on the axisymmetric extrudate swell flow of a viscoelastic material with yield stress (by means of biviscosity formulation) and by Hurez et al. (1990) who employed the augmented Lagrangian method to solve the extrusion flow of Herschel–Bulkley fluids from planar and round dies. Ellwood et al. (1990) reported similar results for the creeping extrudate swell flow from both round and slit dies and presented results for moderate Reynolds numbers and relatively low values of the yield stress. Mitsoulis and co-workers (Abdali et al. 1992; Mitsoulis et al. 1993) showed that in the creeping extrudate swell flow of a Bingham plastic, the extrudate swell ratio is reduced as the yield stress is increased and beyond a certain value, the jet actually contracts slightly reaching a minimum and then starts increasing to reach unity asymptotically. Contraction reaches about 5 % for the planar and about 2 % for the axisymmetric die. The appearance of the minimum at high yield stress values was attributed to the fact that the surrounding yielded layer of the fluid is less viscous than the unyielded plug-flow core. Abdali et al. (1992) also noted that the extrudate contracts when the viscosity ratio is low and the relative radius of the core is close to unity. Hence, inertia is expected to compete yield stress effects at high values of the latter. Moreover, slip is expected to oppose yield stress effects in an intermediate range of yield stress values (where the extrudate contracts but the extrudate swell ratio is still decreasing with yield stress). Belblidia et al. (2009) solved numerically the time-dependent, weakly compressible extrudate swell flow of a Herschel–Bulkley fluid. They reported that extrudate swell is unaltered by compressibility under no-slip wall conditions and noted that this result may be altered by considering wall slip.

The assumption of creeping flow may be valid for a large number of applications with yield stress fluids (Mitsoulis 2007). However, moderate or even high Reynolds numbers are encountered in many important processes, such as oil drilling, and cement and foam flows. To our knowledge, no systematic results have been presented in the literature for the inertia effects in extrudate swell flow of yield stress fluids. Ellwood et al. (1990) reported that as the yield stress increases, swelling at low and contraction at higher Reynolds numbers are reduced, due to the increased tendency for the center core of the jet to exit the die as a solid plug when the yield stress increases. Ellwood et al. (1990) did present free surface profiles of the axisymmetric extrudate for a moderate value of the Reynolds number at which the jet actually contracts. They noted that in this regime necking occurs as the yield stress increases and vanishes if the latter is further increased.

Sochi (2011) notes that wall slip with yield stress fluids is common place while Yilmazer and Kalyon (1989) point out that slip may lead to spectacular effects. The effects of compressibility on the Newtonian extrudate swell flow have been investigated by Beverly and Tanner (1993) and Georgiou (1995) and, more recently, by Taliadorou et al. (2008) and Kountouriotis et al. (2013). Georgiou (2003) studied the compressible extrudate swell flow of a Carreau fluid with nonlinear slip at the wall, in an attempt to simulate the stick–slip extrusion instability. Damianou et al. (2013) compiled experimental works demonstrating slip with yield stress materials as well as numerical works concerning weakly compressible flows of yield stress fluids, such as the transport of waxy crude oils. They also derived approximate semi-analytical solutions of the steady, creeping, weakly compressible plane and axisymmetric Poiseuille flows of a Herschel–Bulkley fluid with slip at the wall. These solutions reveal that when the yield stress fluid is compressible, the upstream velocity tends to become plug, an effect enhanced by slip. In the case of incompressible flow, the velocity becomes plug at a finite critical value of the (inverse) slip parameter which is inversely proportional to the yield stress. This implies that for a given Navier slip coefficient, there is an upper bound for the admissible yield stress of the material and vice versa.

In the present work, we are interested in the position and the shape of the free surface and not in the yielded and unyielded regions in the extrudate swell flow domain. We thus employ the Papanastasiou regularization, following previous works (Papanastasiou 1987; Ellwood et al. 1990; Mitsoulis 2007; Abdali et al. 1992). To our knowledge, the ALM has been used only by Hurez et al. (1990) in solving the extrudate swell flow of Herschel–Bulkley fluids. However, they presented only sample results. The paper can be viewed as an extension of our recent work on the Newtonian extrudate swell problem (Kountouriotis et al. 2013). This is organized as follows. In Governing equations, the governing equations and boundary conditions are presented and then nondimensionalized. To account for wall slip and compressibility effects, we use Navier's slip law (Navier 1827) and an exponential equation of state relating the fluid density to the pressure (Taliadorou et al. 2008). In Numerical results and discussion, the numerical method is briefly described and the numerical results are presented and the effects of the various dimensionless numbers are discussed. Finally, our conclusions are summarized in Concluding remarks.

Governing equations

We consider the steady, creeping, axisymmetric extrudate swell flow of a compressible Herschel–Bulkley fluid neglecting gravity. The continuity equation and momentum equation are as follows:

$$\nabla\cdot(\rho\mathbf{u}) = 0 \tag{4}$$

and

$$\rho(\mathbf{u}\cdot\nabla\mathbf{u}) = -\nabla p + \nabla\cdot\boldsymbol{\tau}, \tag{5}$$

where ρ is the density, and p is the pressure. Under the assumption of zero bulk viscosity, the tensorial form of the constitutive equation of compressible Herschel–Bulkley fluid is given by

$$\begin{cases} \dot{\boldsymbol{\gamma}} = 0, & \tau \le \tau_0 \\ \boldsymbol{\tau} = \left(\dfrac{\tau_0}{\dot{\gamma}} + k\dot{\gamma}^{n-1}\right)\left(\dot{\boldsymbol{\gamma}} - \dfrac{2}{3}\nabla\cdot\mathbf{u}\,\mathbf{I}\right), & \tau > \tau_0 \end{cases} \tag{6}$$

where $\mathbf{I}$ is the identity tensor. In the present work, we use the following Papanastasiou regularization of Eq. (6):

$$\boldsymbol{\tau} = \left[\tau_0\frac{1-\exp\left(-m\dot{\gamma}\right)}{\dot{\gamma}} + k\dot{\gamma}^{n-1}\right]\left(\dot{\boldsymbol{\gamma}} - \frac{2}{3}\nabla\cdot\mathbf{u}\,\mathbf{I}\right) \tag{7}$$

For weakly compressible flows, the fluid density, ρ, can be assumed to vary exponentially with pressure (Wachs et al. 2009):

$$\rho = \rho_0 e^{\beta(p-p_0)}, \tag{8}$$

where ρ_0 is the density at the atmospheric pressure p_0, and β is the isothermal compressibility, assumed to be constant.

The geometry and boundary conditions of the axisymmetric extrudate swell problem are shown in Fig. 1. The radius of the capillary is denoted by R. The standard symmetry conditions for zero radial velocity and shear stress along the axis of symmetry are assumed. Along the capillary wall, the radial velocity is set to zero (no penetration) and the axial velocity obeys Navier's slip condition,

$$\tau_w = \frac{1}{a}u_w, \tag{9}$$

where u_w is the slip velocity, τ_w is the wall shear stress, and a is an inverse slip parameter depending on the material properties for a given wall. When $a=0$, the no-slip boundary condition is recovered. In the case of a nonyield stress fluid, there is no bound on the permissible values of a; in the limit $a\to\infty$, full slip is achieved. As discussed below, in the case of yield stress fluids, there exists an upper bound on the value of a, which depends on the yield stress. Equation (9) and its power-law generalization have been employed by various groups in analyzing slip flows of Herschel–Bulkley fluids (see Aktas et al. (2014) and references therein).

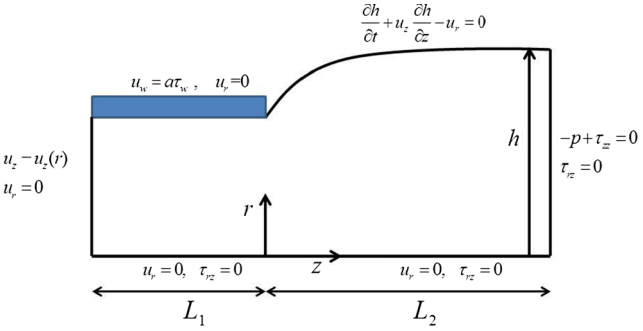

Fig. 1 Geometry and dimensionless boundary conditions for the axisymmetric extrudate swell flow of a compressible Herschel–Bulkley fluid with wall slip

The inlet plane is taken far upstream of the exit at a distance $L_1=20R$ so that the flow can be taken as fully developed, i.e., $u_r=0$ and the axial velocity is given by the standard steady-state axisymmetric Poiseuille flow of a Herschel–Bulkley fluid:

$$u_z(r) = u_w + \frac{nG^{1/n}}{2^{1/n}(n+1)k^{1/n}}\begin{cases} (R-r_0)^{1/n+1}, & 0\le r\le r_0 \\ \left[(R-r_0)^{1/n+1} - (r-r_0)^{1/n+1}\right], & r_0\le r\le R \end{cases} \tag{10}$$

where $G\equiv(-dp/dz)$ is the imposed pressure gradient, u_w is the slip velocity, given by

$$u_w = \frac{aRG}{2} \tag{11}$$

and r_0 is the yield point:

$$r_0 = \frac{2\tau_0}{G} < R \tag{12}$$

It should be noted that there is no flow when the pressure gradient is below $2\tau_0/R$.

The outlet plane is taken at a distance $L_2=50R$ from the exit so that the flow can be considered uniform. Hence, under the assumption of zero surface tension the total normal stress and the shear stress vanish, $-p+\tau_{zz}=0$ and $\tau_{rz}=0$. Finally, on the free surface, vanishing normal and tangential stresses are imposed along with the kinematic condition:

$$\frac{\partial h}{\partial t} + u_z\frac{\partial h}{\partial z} - u_r = 0 \tag{13}$$

This last equation is in fact used in order to calculate the unknown position $h=h(z)$ of the free surface (full-Newton iteration).

Nondimensionalization

The governing equations are nondimensionalized by scaling the lengths by the radius R of the tube, the velocity vector by the mean velocity U at the inlet of the tube, the pressure and the stress tensor components by kU^n/R^n, and the density by ρ_0. The dimensionless forms of the continuity and momentum equations are

$$\nabla^*\cdot\left(\rho^*\mathbf{u}^*\right)=0 \tag{14}$$

and

$$\rho^* Re\left(\mathbf{u}^*\cdot\nabla^*\mathbf{u}^*\right)=-\nabla^* p^*+\nabla^*\cdot\boldsymbol{\tau}^*, \tag{15}$$

where the stars denote dimensionless variables and

$$Re\equiv\frac{\rho U^{2-n}R^n}{k} \tag{16}$$

is the Reynolds number. The equation of state (8) becomes:

$$\rho^*=e^{Bp^*}, \tag{17}$$

where B is the compressibility number:

$$B\equiv\frac{\beta k U^n}{R^n} \tag{18}$$

Similarly, the dimensionless form of the Papanastasiou-regularized constitutive equation is

$$\boldsymbol{\tau}^*=\left[Bn\frac{1-\exp\left(-M\dot{\gamma}^*\right)}{\dot{\gamma}^*}+\dot{\gamma}^{*n-1}\right]\left(\dot{\boldsymbol{\gamma}}^*-\frac{2}{3}\nabla\cdot\mathbf{u}^*\mathbf{I}\right) \tag{19}$$

where

$$Bn\equiv\frac{\tau_0 R^n}{kU^n} \tag{20}$$

is the Bingham number and

$$M\equiv\frac{mU}{R} \tag{21}$$

is the dimensionless growth exponent.

The dimensionless velocity profile imposed at the inlet is

$$u_z^*(r)=u_w^*+\frac{nG^{*1/n}}{2^{1/n}(n+1)}\begin{cases}\left(1-r_0{}^*\right)^{1/n+1}, & 0\le r^*\le r_0{}^*\\ \left[\left(1-r_0{}^*\right)^{1/n+1}-\left(r-r_0{}^*\right)^{1/n+1}\right], & r_0{}^*\le r^*\le 1\end{cases} \tag{22}$$

where

$$r_0{}^*=\frac{2Bn}{G^*}<1 \tag{23}$$

and the dimensionless pressure gradient is the root of the following equation

$$2^{1/n}\frac{3n+1}{n}\left(1-u_w^*\right)G^{*3}=\left(G^*-2Bn\right)^{1/n+1}\left[G^{*3}+\frac{4nBn}{2n+1}G^*+\frac{8n^2Bn^2}{(n+1)(2n+1)}\right] \tag{24}$$

which is obtained by demanding that the dimensionless volumetric flow rate is $Q^*=\pi$.

The dimensionless form of the slip equation is

$$u_w{}^*=A\tau_w^* \tag{25}$$

where

$$A\equiv\frac{kaU^{n-1}}{R^n} \tag{26}$$

is the slip number. It is important to note that for a given slip number, there is an upper bound for the Bingham number, which cannot be exceeded. This limiting value corresponds to the pressure gradient at which the fluid yields. From Eqs. (24)–(26), it is easily deduced that when Bn is equal to $Bn_{crit}=1/A$, both r_0^* and u_w^* become 1 (Damianou et al. 2013). Similarly, for a given Bingham number, the slip number should not exceed $1/Bn$.

Numerical results and discussion

The finite element method is used for solving the system of governing equations and boundary conditions presented in Governing equations. The free surface profile is computed simultaneously with the velocity and pressure fields (*u-v-p-h* formulation), and the mesh is updated at each iteration step by means of a spine scheme. Standard biquadratic basis functions are used for the two velocity components and bilinear ones for the pressure field, while the unknown position of the free surface, h, is approximated by quadratic basis functions. The standard Galerkin forms of the continuity, momentum, and kinematic equations are used. The nonlinear system of equations is solved with the Newton–Raphson iterative scheme with a convergence tolerance equal to 10^{-4}. All the numerical

simulations in this section concern the steady-state axisymmetric flow of a Herschel–Bulkley fluid. The lengths of the die and the extrudate (L_1^*=20 and L_2^*=50) are considered sufficient for the range of *Re* examined (0–100). Finite element meshes of different refinements have been used in order to ensure the convergence of the numerical solutions.

When using a regularized constitutive equation, such as the Papanastasiou model, converged results can be obtained only up to a critical value, M_c, of the growth exponent, which depends on the flow parameters and mesh refinement. In our simulations of incompressible flow, $M_c \geq 500$ for $Bn \leq 20$. For some moderate and high Bingham numbers, $M_c \geq 300$, depending on the values of *Re* and *A*. Some points in the range $50 < Bn < 100$, used in constructing plots of the extrudate swell ratio versus the Bingham number, were calculated with $M_c \geq 100$.

We first studied the combined effects of yield stress and inertia on the extrudate surface in the case of Bingham flow (n=1) with no wall slip. Figure 2 shows free surfaces obtained for *Re*=0, 1, and 10 and various Bingham numbers in the range [0, 100], which is much larger than the range [0, 1] covered by Ellwood et al. (1990). According to Mitsoulis (2007), most of the interesting viscoplastic phenomena occur for $1 < Bn < 10$. As already discussed, in creeping flow (Fig. 2a), swelling is reduced as the Bingham number is increased and beyond a critical Bingham number, the jet actually contracts till a minimum (roughly at Bn=10 for n=1) beyond which the extrudate swell ratio goes asymptotically to unity (Abdali et al. 1992; Mitsoulis 2007). The results for *Re*=1 are similar (Fig. 2b); swelling at low values of *Bn* is actually less than that for the creeping case and the differences diminish as the Bingham number is increased (see Fig. 3a). The fact that inertia reduces swelling in the case of a Newtonian jet and beyond a critical Reynolds number the jet actually contracts is well known (Georgiou et al. 1988; Taliadorou et al. 2008). Nevertheless, the present results show that in the case of Bingham flow inertia enhances swelling initially and only beyond a critical number swelling is reduced. In Fig. 2c (*Re*=10), we observe that the extrudate contracts when *Bn*=0 (Newtonian fluid). More precisely, the extrudate contracts only for a small distance after the die exit and then expands slightly so that the extrudate swell ratio is less than unity. When the Bingham number is increased, the initial contraction is reduced while the expansion downstream becomes more pronounced, resulting in the appearance of necking. At higher Bingham numbers, the extrudate swell ratio actually exceeds unity, i.e., the extrudate swells, while the neck becomes less severe. However, beyond a critical Bingham number, swelling starts reducing and contraction is observed again up to a critical Bingham number beyond which the jet expands again and the extrudate swell ratio tends asymptotically to unity.

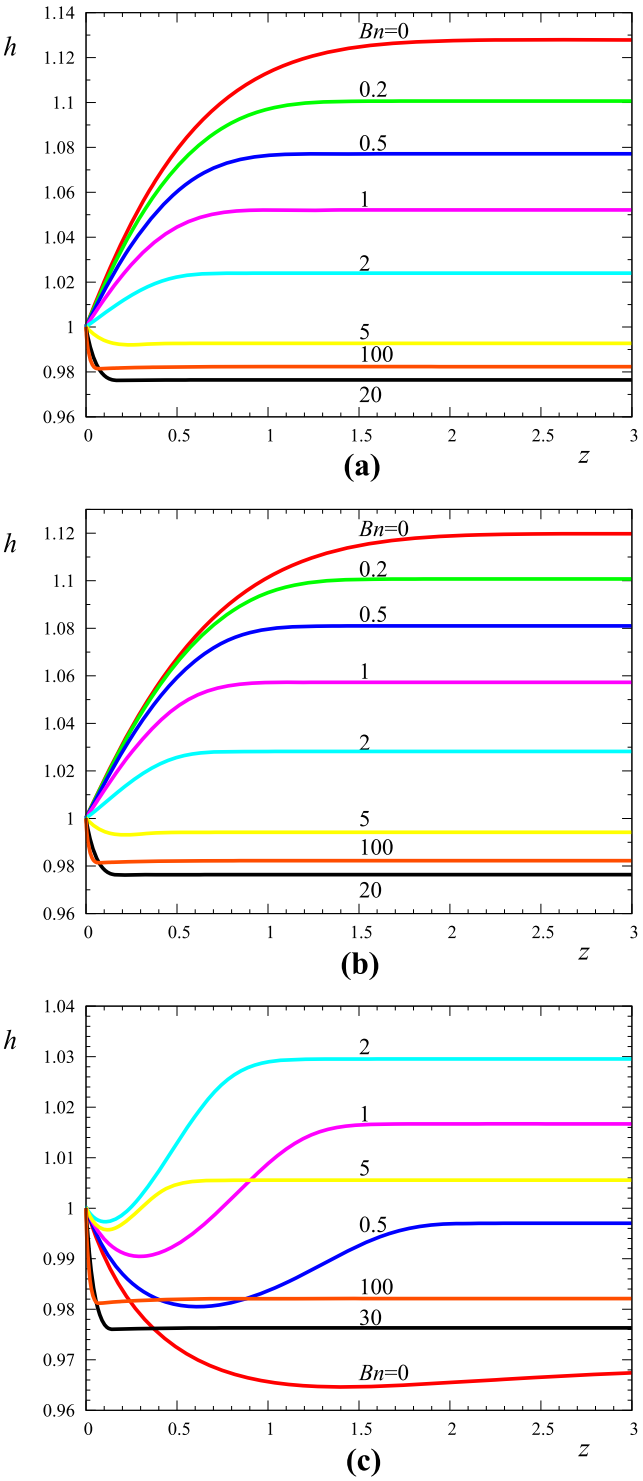

Fig. 2 Free surface profiles in incompressible (B=0) Bingham flow (n=1) for A=0 (no slip) and various Bingham numbers: **a** *Re*=0, **b** *Re*=1, and **c** *Re*=10

The variation of the extrudate swell ratio with the Bingham number is illustrated in Fig. 3a, where the results for *Re*=0, 1, 5, and 10 are shown. The results for *Re*=0 coincide with those of Abdali et al. (1992) who used a different definition for the Bingham number (Bi=2*Bn*). As indicated by one of the

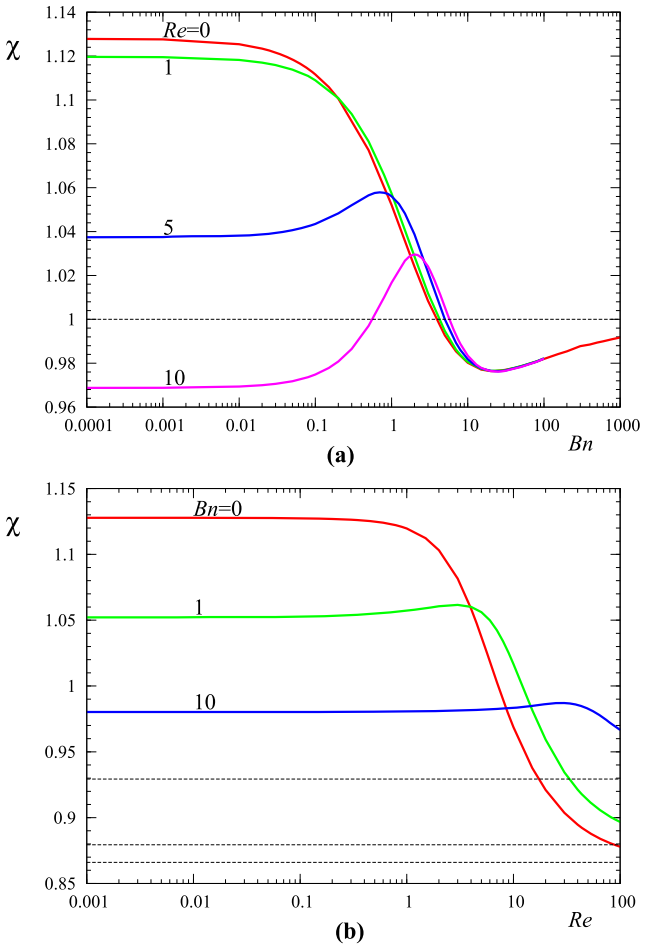

Fig. 3 **a** Extrudate swell ratios in Bingham flow with Re=0, 1, 5, and 10; **b** Extrudate swell ratios in Bingham flow with Bn=0, 1, and 10; the *dotted lines* indicate the asymptotic limits for infinite Reynolds number

referees, the flow at large Bingham numbers just inside the tube is close to being a rod of radius 1-Δh with a shear layer of thickness Δh. Due to the conservation of mass the jet radius far downstream must be 1-Δh/2, i.e., the jet contraction is Δh/2. It is then clear that contraction tends to zero as the Bingham number and/or the slip number are increased. For moderate Reynolds numbers, the extrudate swell ratio increases with the Bingham number to reach a global maximum (above unity) and then a local minimum (below unity) before converging to unity. At higher Reynolds numbers, the maximum of the extrudate swell ratio is expected to correspond to contraction (χ<1); however, carrying out such simulations is outside the scope of the present work. Figure 3b shows the variation of the extrudate swell ratio for Bn= 0, 1, and 10 versus the Reynolds number. This decreases monotonically only in the Newtonian case (Bn=0) reaching the asymptotic value 0.8660 (Kountouriotis et al. 2013; Ellwood et al. 1990). When the Bingham number is nonzero, the extrudate swell ratio initially increases slightly reaching a maximum (above unity) which is shifted to the right as the Bingham number is increased. This trend is followed even when the extrudate contracts which is the case for Bn= 10. After the maximum the extrudate swell ratio

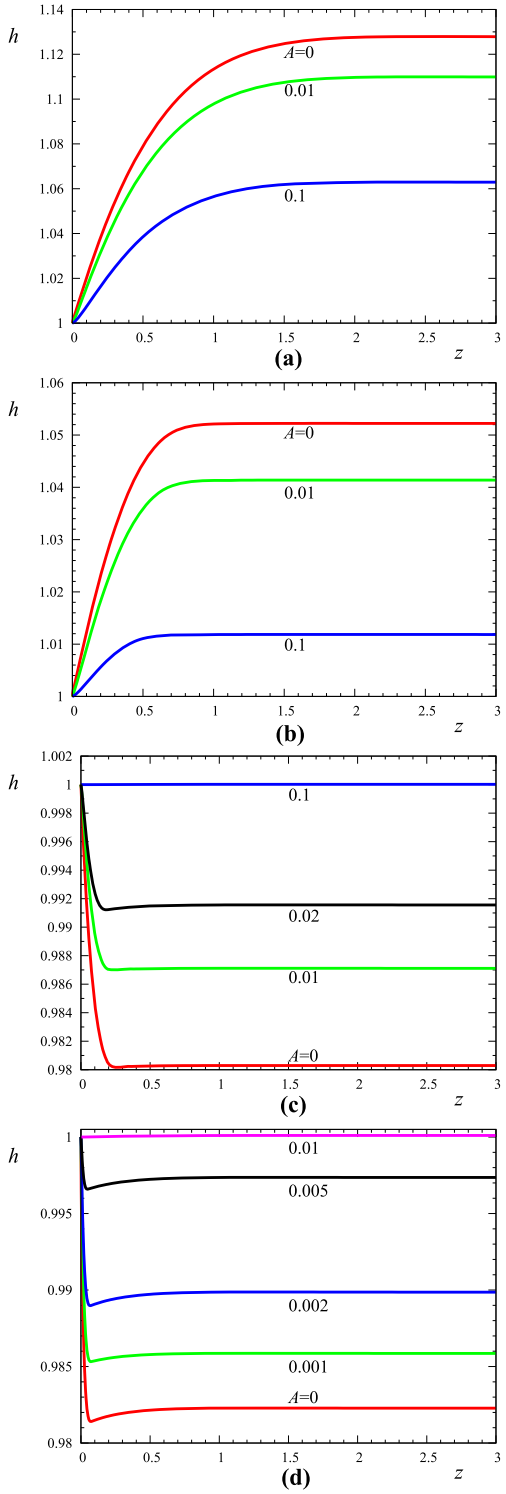

Fig. 4 Free surface profiles in incompressible (B=0) Bingham flow (n= 1) for Re=0 and various slip numbers: **a** Bn=0, **b** Bn=1, **c** Bn=10, and **d** Bn=100

decreases monotonically reaching the corresponding asymptotic value. This value increases with the Bingham number from 0.8660 ($Bn=0$) to unity (infinite Bn). The asymptotic extrudate swell ratio has been derived by Ellwood et al. (1990). Using the notation of the present paper, this is given by

$$\chi_\infty \equiv \frac{4\sqrt{15}}{\left(2Bn/G^*-1\right)^2\sqrt{16Bn^2+12BnG^*+5G^{*2}}} \tag{27}$$

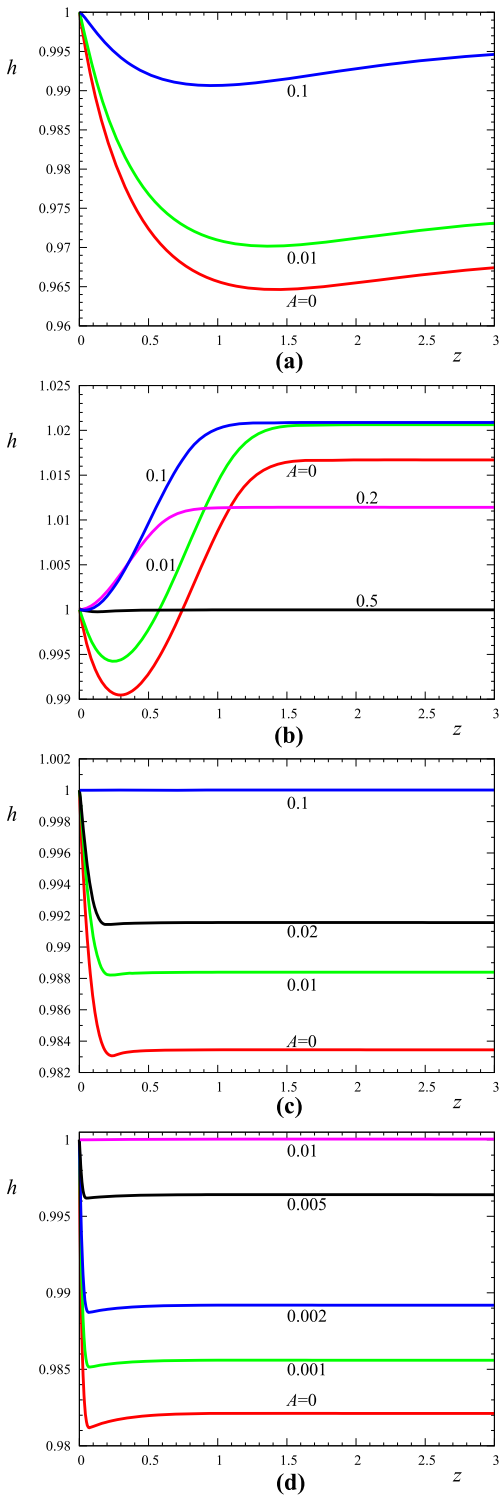

Fig. 5 Free surface profiles in incompressible ($B=0$) Bingham flow ($n=1$) for $Re=10$ and various slip numbers: **a** $Bn=0$, **b** $Bn=1$, **c** $Bn=10$, and **d** $Bn=100$

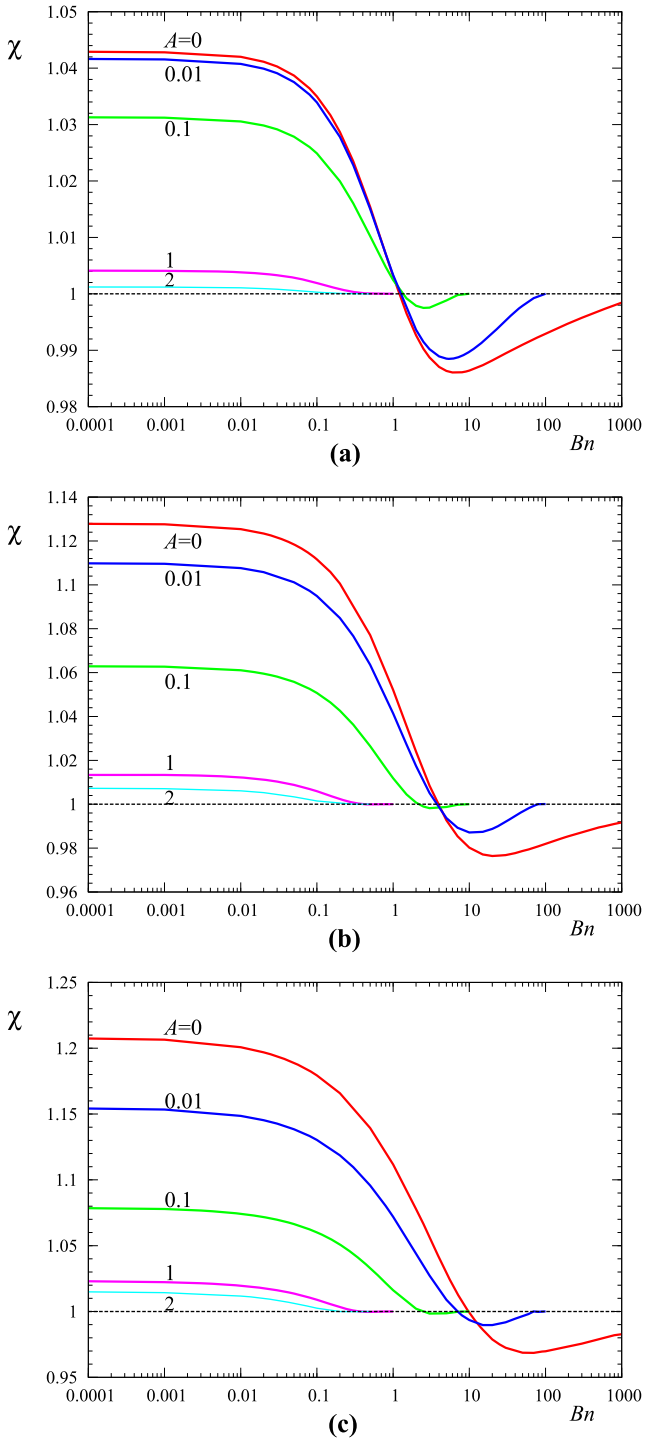

Fig. 6 Extrudate swell ratios in incompressible ($B=0$), creeping ($Re=0$) Herschel–Bulkley flow: **a** $n=0.5$, **b** $n=1$, and **c** $n=1.5$. Note that the y-scale is not the same in all graphs

where G^* is the largest root of

$$3G^{*4} - 8(Bn+3)G^{*3} + 16Bn^4 = 0 \quad (28)$$

The effect of slip on the incompressible extrudate swell flow of a Bingham fluid (n=1) was studied next. It is well established that in the Newtonian case, slip reduces swelling at low and contraction at higher Reynolds numbers (Kountouriotis et al. 2013). As illustrated in Fig. 4, where free surfaces for the creeping flow obtained for different Bingham and slip numbers are shown, in the case of Bingham flow, slip reduces swelling at low and contraction at high Bingham

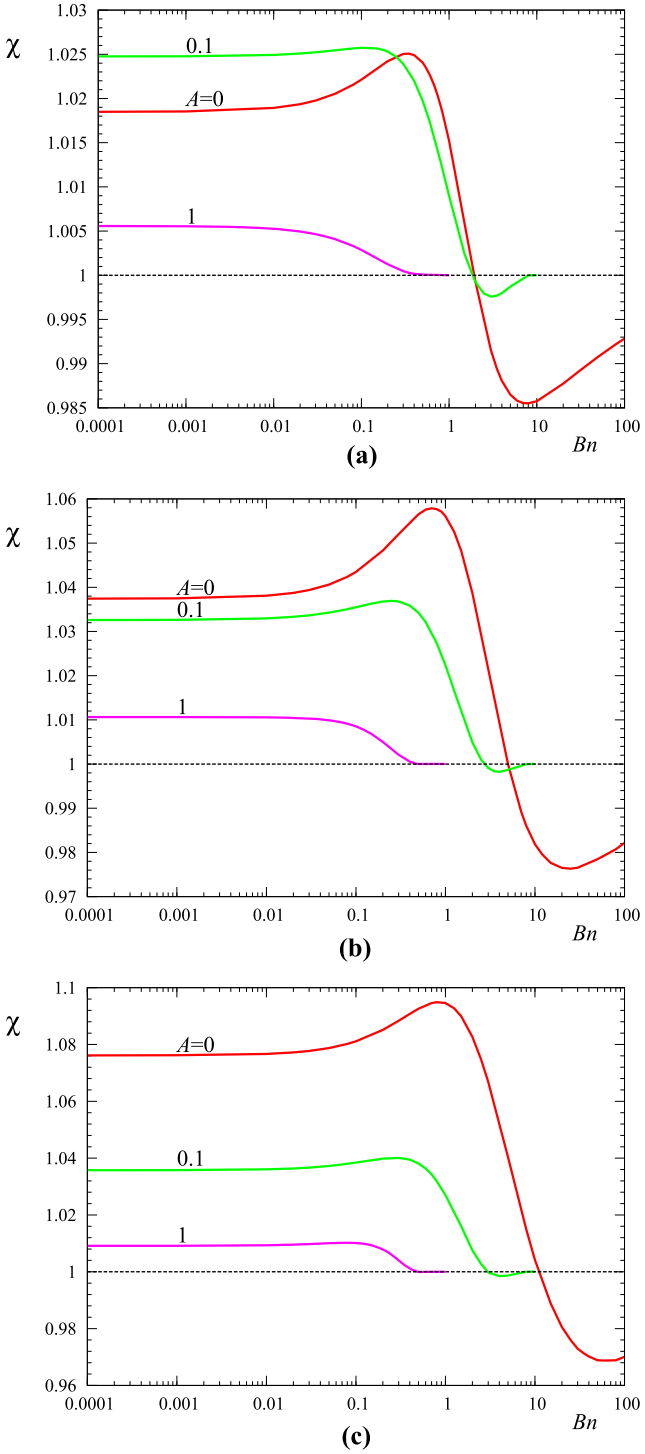

Fig. 7 Extrudate swell ratios in incompressible (B=0) Herschel–Bulkley flow for Re=5: **a** n=0.5, **b** n=1, and **c** n=1.5. Note that the y-scale is not the same in all graphs

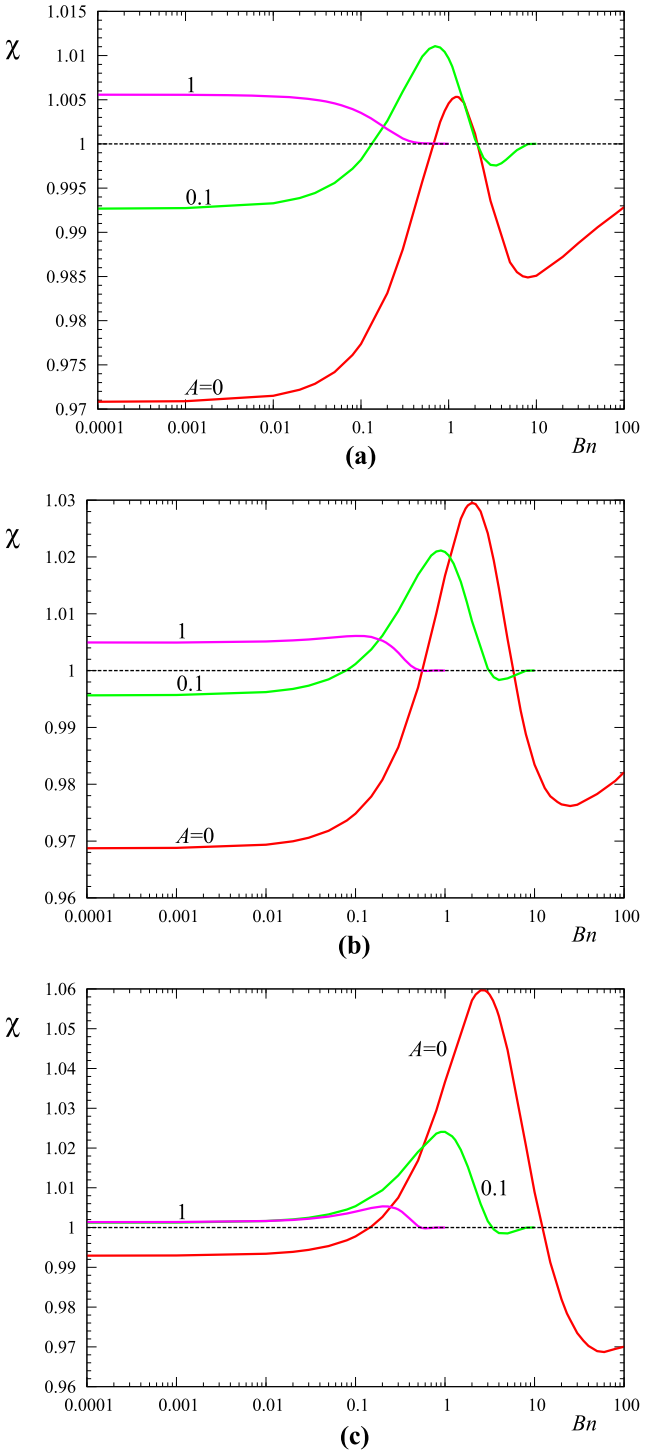

Fig. 8 Extrudate swell ratios in incompressible (B=0) Herschel–Bulkley flow for Re=10: **a** n=0.5, **b** n=1, and **c** n=1.5. Note that the y-scale is not the same in all graphs

numbers. At intermediate values of the Reynolds number, i.e., for Re=10 (Fig. 5), slip reduces contraction at low and high Bingham numbers. In the intermediate regime in which the jet exhibits necking, slip may initially result in further swelling and the elimination of the necking. Eventually, however, when slip becomes stronger, swelling is suppressed and the extrudate tends to become cylindrical.

The effect of slip on the incompressible, creeping (Re=0) extrudate swell flow of a Herschel–Bulkley fluid was studied for three values of the power-law exponent: n=0.5, 1, and 1.5.

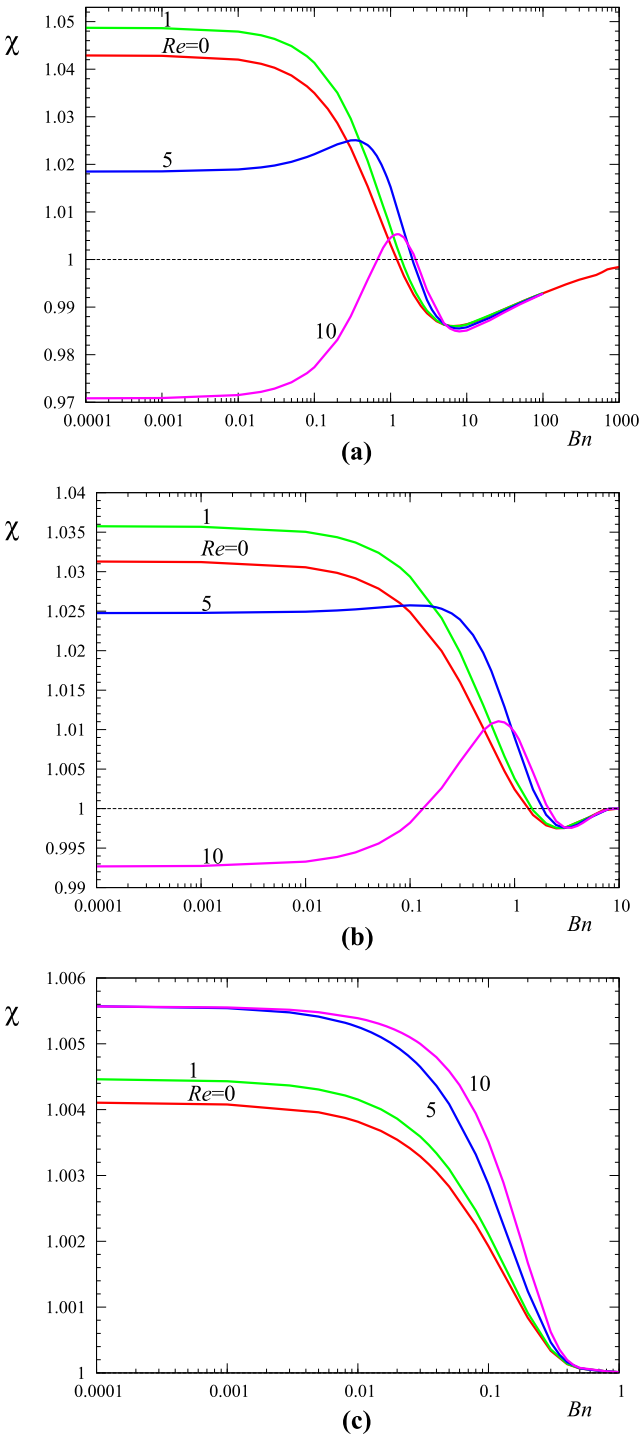

Fig. 9 Extrudate swell ratios in incompressible (B=0) Herschel–Bulkley flow with n=0.5 for various Reynolds numbers: **a** A=0 (no slip), **b** A=0.1 (moderate slip), and **c** A=1 (strong slip). Note that the y-scale is not the same in all graphs

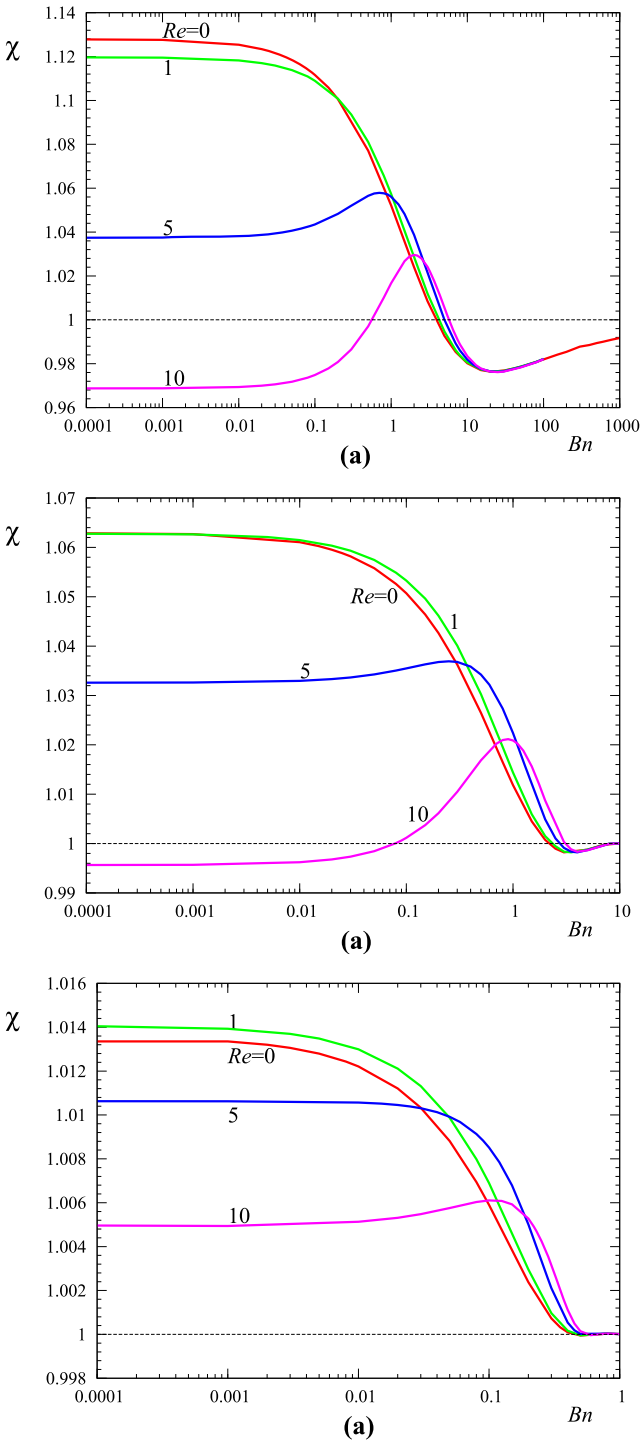

Fig. 10 Extrudate swell ratios in incompressible (B=0) Bingham flow (n=1) for various Reynolds numbers: **a** A=0 (no slip), **b** A=0.1 (moderate slip), **c** A=1 (strong slip). Note that the y-scale is not the same in all graphs

In Fig. 6, the calculated extrudate swell ratios for five different slip numbers (A=0, 0.01, 0.1, 1, and 2) are plotted versus the Bingham number up to the corresponding critical value $Bn_{crit}=1/A$. It is well established that swelling increases with the power-law index (Huynh 1982; Mitsoulis 2007). From Fig. 6, it is deduced that the contraction of the extrudate at higher Bingham numbers also increases with the power-law index. We observe again that slip reduces swelling at low and contraction at higher Bn. In the presence of slip, contraction is observed at lower Bingham numbers. When slip is strong,

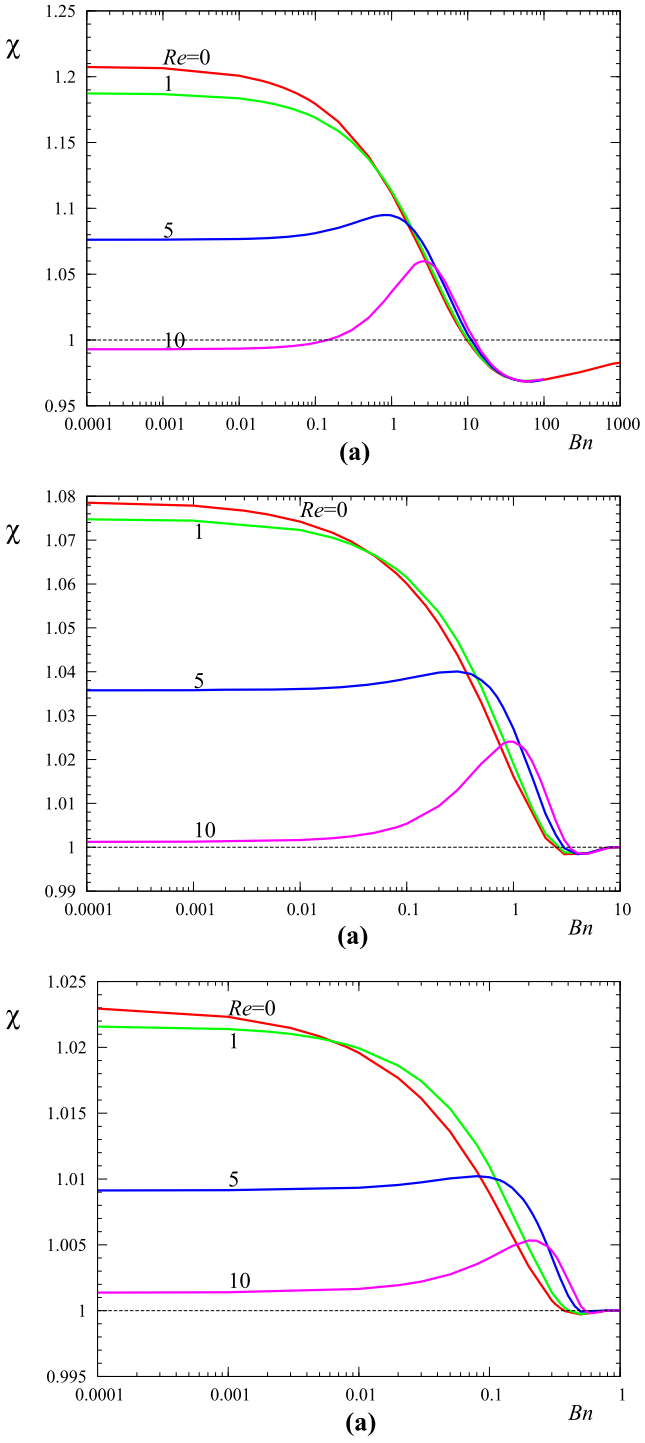

Fig. 11 Extrudate swell ratios in incompressible (B=0) Herschel–Bulkley flow with n=1.5 for various Reynolds numbers: **a** A=0 (no slip), **b** A=0.1 (moderate slip), **c** A=1 (strong slip). Note that the y-scale is not the same in all graphs

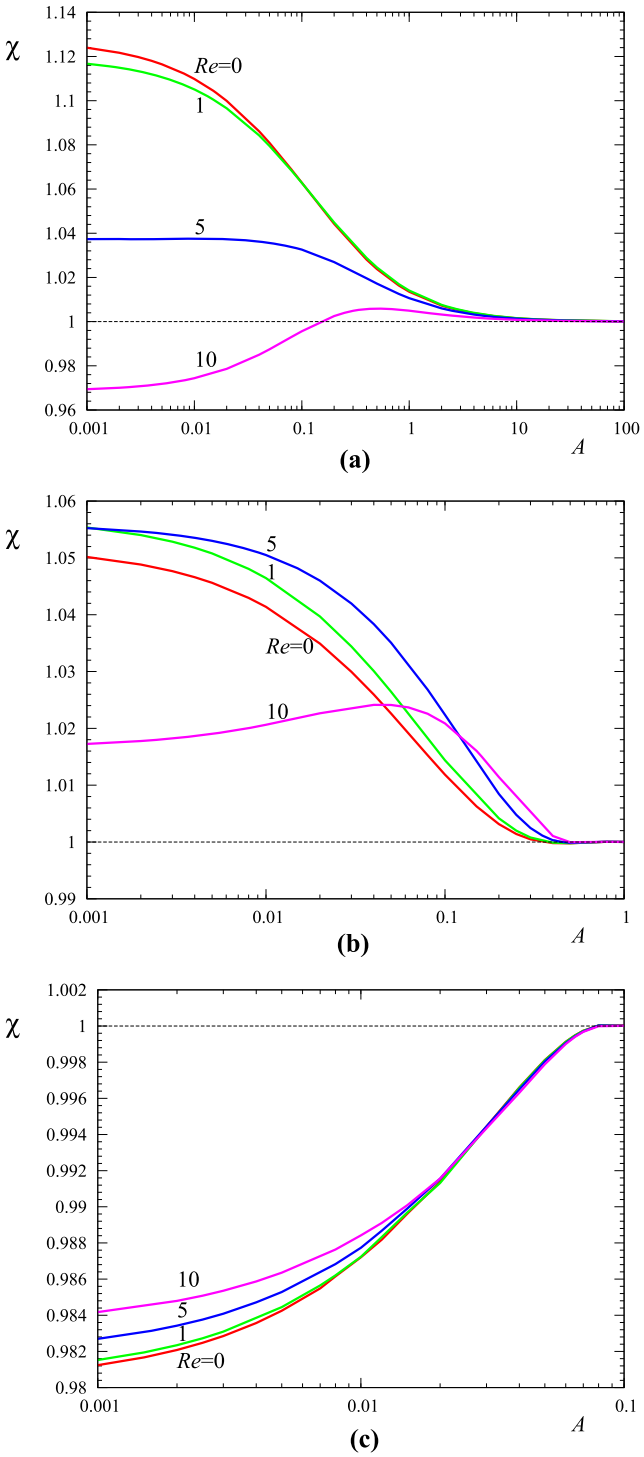

Fig. 12 Extrudate swell ratios in incompressible (B=0) Bingham flow (n=1) for various Reynolds numbers: **a** Bn=0, **b** Bn=1, and **c** Bn=10. Note that the y-scale is not the same in all graphs

swelling is suppressed quickly and no contraction is observed. As the power-law index is increased, swelling is also increased along with the value of the critical Bingham number at which the extrudate swell becomes essentially 1.

In addition to the creeping flow results of Fig. 6, we have carried out simulations for low and moderate values of the Reynolds number. The calculated extrudate swell ratios for Re=5 and 10, the three representative power-law exponents and different slip numbers are shown in Figs. 7 and 8, respectively. Comparing the results of Figs. 6, 7, and 8, we observe that inertia reduces the range of the extrudate swell ratios and postpones contraction at slightly higher Bingham numbers. The results for Re=5 and 10 reveal that slip and inertia effects are competing. In general, swelling and contraction are reduced further; however, in these two cases, the extrudate swell ratio increases initially with the Bingham number reaching a maximum which moves to the right as the power-law exponent is increased. Interestingly, for Re=5 and n=0.5 (shear-thinning fluid), the extrudate swell ratio initially increases with slip (Fig. 7a). This is also the case when Re=10, the jet actually contracts at least for low Bingham numbers, as illustrated in Fig. 8. The contraction of the jet is reduced with slip and the jet actually expands when slip becomes strong.

The competition between slip and inertia for n=0.5, 1, and 1.5 is also illustrated in Figs. 9, 10, and 11, where the extrudate swell ratios obtained with A=0 (no slip), 0.1 (moderate slip), and 1 (strong slip), and Re=0, 1, 5, and 10 are plotted versus the Bingham number. It should be noted that the extrudate swell ratio of the shear-thinning fluid initially increases with the Reynolds number. When slip is strong (A=1), the extrudate swell ratio increases for all the Reynolds numbers examined. In the case of the Bingham flow (Fig. 10), the extrudate swell ratio decreases with the Reynolds number only when both the Bingham and slip numbers are low. The extrudate swell ratios are plotted versus the slip number in Fig. 12 for different Bingham and Reynolds numbers.

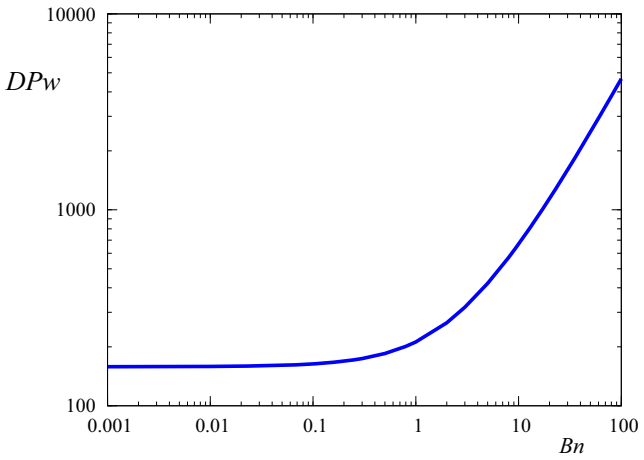

Fig. 13 Pressure drop in incompressible Bingham flow with no wall slip; B=0, n=1, A=0, and L_1=20

The present simulations are general in the sense that we have not considered any specific material. In order to investigate compressibility effects, we carried out simulations for small compressibility numbers, e.g., of the order 10^{-3} to 10^{-5},

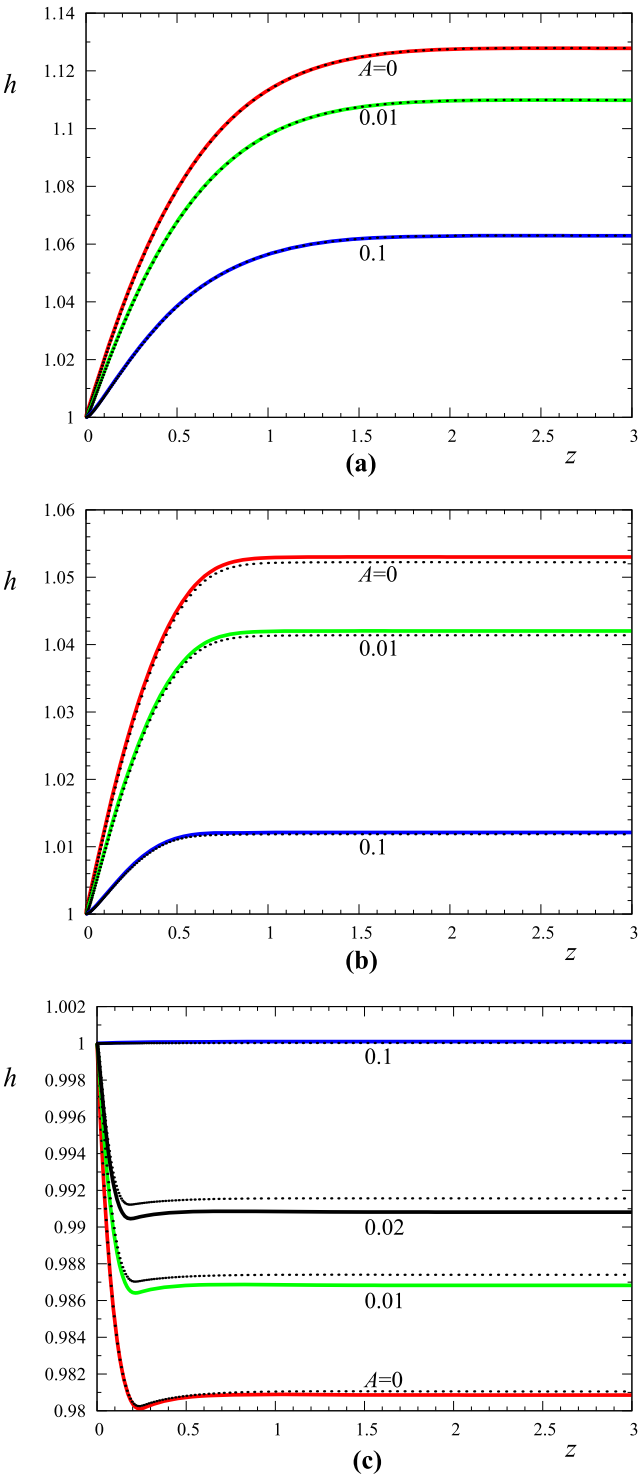

Fig. 14 Free surface profiles in compressible creeping Bingham flow (n=1) for B=0.0001 and various slip numbers: **a** Bn=0, **b** Bn=1, and **c** Bn=10. The *dotted lines* indicate the corresponding results for incompressible flow

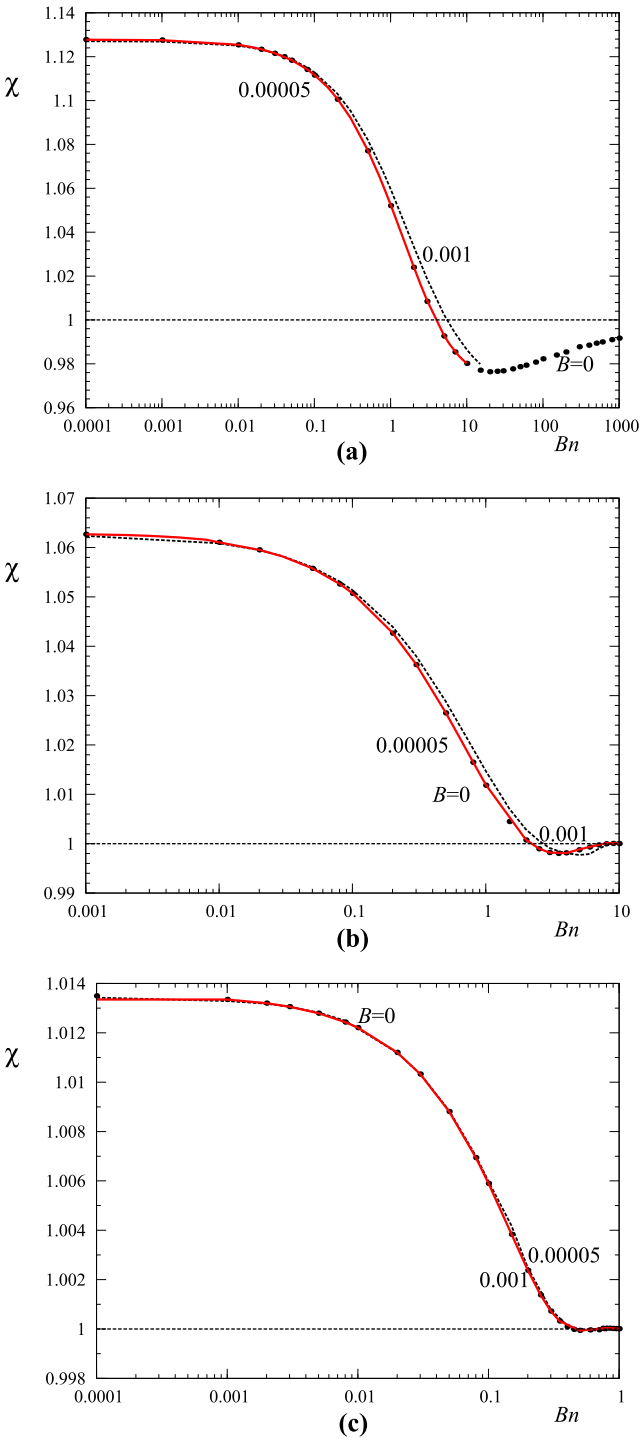

Fig. 15 Extrudate swell ratios for Bingham flow (n=1) with Re=0 and B=0 (*bullets*), 0.00005 (*solid*), and 0.001 (*dashed*): **a** A=0 (no slip), **b** A=0.1 (moderate slip), and **c** A=1 (strong slip)

with $M_c \geq 500$ for $Bn \leq 20$ and $M_c \geq 100$ for Bn=100. These values of the compressibility number are consistent, for example, with the values reported by Vinay et al. (2006) for waxy crude oils in pipelines. The latter authors noted that the order of magnitude of BRe usually varies from 10^{-9} to 10^{-3}.

As expected, the pressure drop required to drive the extrudate swell flow of a viscoplastic material increases rapidly with yield stress. As illustrated in Fig. 13, where the pressure drop for creeping incompressible Bingham flow with no wall slip is plotted versus the Bingham number, for Bn>1, increasing Bn by one order of magnitude raises the required pressure drop by an order of magnitude too. This increase may be even more dramatic in the case of a longer die. Such dramatic increases of the pressure would then lead to dramatic density changes not admissible for liquid and viscoplastic materials, which cause the divergence of the numerical code.

The effect of compressibility is illustrated in Fig. 14, where free surface profiles for the compressible (B=0.0001) creeping (Re=0) flow of a Bingham plastic with different Bingham and slip numbers are plotted (similar results have been obtained for B=0.00005). The dotted lines show the corresponding results for the incompressible flow (B=0). As expected, for a Newtonian fluid (Fig. 14a), weak compressibility (B=0.0001) has no effect on extrudate swell. It is well known in the literature that in creeping flow (Re=0), increasing compressibility initially leads to a small reduction of the extrudate swell ratio and then enhances swelling but this effect can only be realized when much higher values of B are considered (Silliman and Scriven 1980; Kountouriotis et al. 2013; Mitsoulis et al. 2012). For Bn=1, compressibility tends to increase swelling, while for Bn=10, compressibility enhances the contraction of the jet, especially at moderate slip numbers. Obviously, this effect is opposite to that of slip, which prevails as the slip number is increased.

In Fig. 15, we plotted the extrudate swell ratios calculated with A=0, 0.1, and 1 (corresponding to no slip, moderate slip, and strong slip, respectively) and B=0, 0.00005, and 0.001. The latter value of the compressibility number is rather unrealistic; this was chosen simply in order to enhance compressibility effects. We observe that compressibility tends to increase the extrudate swell ratio for Bingham numbers in the range [0.1, 10], especially when slip is not strong.

Concluding remarks

The axisymmetric extrudate swell flow of a compressible Herschel–Bulkley fluid was solved numerically using the Papanastasiou-regularized version of the constitutive equation. The effects of yield stress, inertia, slip, and compressibility on the free surface shape and the extrudate swell-ratio have been studied. For that purpose, Navier's slip condition and an exponential equation of state relating the density to the pressure have been employed.

For low Reynolds numbers, the extrudate swell ratio, χ, initially decreases with the Bingham number reaching a minimum corresponding to contraction and then increases asymptotically to unity. For moderate Reynolds numbers, however,

χ initially increases with the Bingham number reaching a maximum after which yield stress effects prevail and the behavior of χ is similar to that at low Reynolds numbers. As a consequence of the competition between inertia and yield stress effects, χ is not a strictly decreasing function of the Reynolds number; it initially increases slightly with *Re* reaching a maximum which is shifted to the right as *Bn* is increased. Inertia is found to reduce the range of attainable extrudate swell ratios and delays the contraction of the extrudate at higher Bingham numbers. Increasing the power-law index enhances swelling at low and contraction at moderate values of the Bingham number.

When the Reynolds number is low, slip suppresses both swelling and contraction of the extrudate, depending on the value of the Bingham number. For moderate Reynolds numbers at which the extrudate exhibits necking, slip tends to eliminate necking and may initially cause further swelling of the extrudate, which is suppressed if slip becomes stronger.

The simulations for the compressible flow indicate that an ideal viscoplastic material even with a moderate yield stress can be only weakly compressible, since high pressure requirements result in unrealistically high values of the density, even in short dies. Compressibility tends to increase swelling, especially when slip is not strong and the yield stress is moderate.

Acknowledgments We are grateful to the referees for their constructive comments and criticism. The project was partially funded by the Greek State (Thales project "Covisco", MIS 380238). EM is indebted to the ERASMUS program (subprogram SOCRATES) for scientific visits to Cyprus related to this work.

References

Abdali SS, Mitsoulis E, Markatos NC (1992) Entry and exit flows of Bingham fluids. J Rheol 36:389–407

Aktas S, Kalyon DM, Marín-Santibáñez, Pérez-González J (2014) Shear viscosity and wall slip behavior of a viscoplastic hydrogel. J Rheol 58:513–534

Balmforth NJ, Frigaard IA, Ovarlez G (2014) Yielding to stress: recent developments in viscoplastic fluid mechanics. Annu Rev Fluid Mech 46:121–146

Belblidia F, Haroon T, Webster MF (2009) The dynamics of compressible Herschel–Bulkley fluids in die-swell flows. In: Boukharouda T et al. (eds) Damage and fracture mechanics: failure analysis of engineering materials and structures. Springer, New York, p 425–434

Beverly CR, Tanner RI (1989) Numerical analysis of extrudate swell in viscoelastic materials with yield stress. J Rheol 33:989–1009

Beverly CR, Tanner RI (1993) Compressible extrudate swell. Rheol Acta 32:526–531

Bingham EC (1922) Fluidity and Plasticity. McGraw-Hill, New York

Damianou Y, Georgiou GC, Moulitsas I (2013) Combined effects of compressibility and slip in flows of a Herschel-Bulkley fluid. J Non-Newtonian Fluid Mech 193:89–102

Dimakopoulos Y, Pavlidis M, Tsamopoulos J (2013) Steady bubble rise in Herschel-Bulkley fluids and comparision of predictions via the Augmented Lagrangian Method with those via the Papanastasiou model. J Non-Newtonian Fluid Mech 200:34–51

Ellwood KRJ, Georgiou GC, Papanastasiou TC, Wilkes JO (1990) Laminar jets of Bingham plastic liquids. J Rheol 34:787–812

Fortin M, Glowinski R (1983) Augmented Lagrangians: application to the numerical solution of boundary value problems. North Holland, Amsterdam, The Netherlands

Frigaard IA, Nouar C (2005) On the usage of viscosity regularization methods for visco-plastic fluid flow computation. J Non-Newtonian Fluid Mech 127:1–26

Georgiou GC (1995) The compressible Newtonian extrudate-swell problem. Int J Numer Meth Fl 20:255–261

Georgiou GC (2003) The time-dependent, compressible Poiseuille and extrudate-swell flows of a Carreau fluid with slip at the wall. J Non-Newtonian Fluid Mech 109:93–114

Georgiou GC, Boudouvis AG (1999) Converged solutions of the Newtonian extrudate-swell problem. Int J Numer Methods Fluids 29:363–371

Georgiou GC, Papanastasiou TC, Wilkes JO (1988) Laminar jets at high Reynolds and high surface tension. AIChE J 34:1559–1562

Glowinski R, Wachs A (2011) On the numerical simulation of viscoplastic fluid flow. In: Glowinski R, Xu J (eds) Numerical methods for non-Newtonian fluids, vol 16. Handbook of numerical analysis, Elsevier, pp 483–717

Hurez P, Tanguy PA, Bertrand FH (1990) A finite element analysis of die swell with pseudoplastic and viscoplastic fluids. Comput Method Appl M 86:87–103

Huynh BP (1982) Some finite element studies of extrusion. J Non-Newtonian Fluid Mech 13:1–20

Kountouriotis Z, Georgiou GC, Mitsoulis E (2013) On the combined effects of slip, compressibility, and inertia on the Newtonian extrudate-swell flow problem. Comput Fluids 71:297–305

Mitsoulis E (2007) Flows of viscoplastic materials: models and computation. Rheol Rev 2007:135–178

Mitsoulis E, Abdali SS, Markatos NC (1993) Flow simulation of Herschel–Bulkley fluids through extrusion dies. Can J Chem Eng 71:147–160

Mitsoulis E, Georgiou GC, Kountouriotis Z (2012) A study of various factors affecting Newtonian extrudate swell. Comput Fluids 57: 195–207

Navier CLMH (1827) Sur les lois du mouvement des fluides. Mem Acad R Sci Inst Fr 6:389–440

Omodei BJ (1980) On the die swell of an axisymmetric Newtonian jet. Comput Fluids 8:275–289

Papanastasiou TC (1987) Flows of materials with yield. J Rheol 31:385–404

Rabideau BD, Moucheront P, Bertrand F, Rodts S, Roussel N, Lanos C, Coussot P (2010) The extrusion of a model yield stress fluid imaged by MRI velocimetry. J Non-Newtonian Fluid Mech 165:394–408

Silliman WJ, Scriven LE (1980) Separating flow near a static contact line: slip at a wall and shape of a free surface. J Comp Physiol 34:287–313

Sochi T (2011) Slip at fluid–solid interface. Polym Rev 51:309–340

Taliadorou E, Georgiou GC, Mitsoulis E (2008) Numerical simulation of the extrusion of strongly compressible Newtonian liquids. Rheol Acta 47:49–62

Vinay G, Wachs A, Agassant JF (2006) Numerical simulation of weakly compressible Bingham flows: the restart of pipeline flows of waxy crude oils. J Non-Newtonian Fluid Mech 136:93–105

Wachs A, Vinay G, Frigaard I (2009) A 1.5D numerical model for the start up of weakly compressible flow of a viscoplastic and thixotropic fluid in pipelines. J Non-Newtonian Fluid Mech 159:81–94

Yilmazer U, Kalyon DM (1989) Slip effects in capillary and parallel disk torsional flows of highly filled suspensions. J Rheol 33:1197–1212